

A Conflict-Aware Extension of the Cell Transmission Model for Consistent Intersection Delay Simulation

Zachary Feinstein^a, Justin Plückebaum^{b,*}, Stefan Weber^b

^a*Stevens Institute of Technology, School of Business, Hoboken, NJ 07030, USA*

^b*Leibniz Universität Hannover, House of Insurance & Institute of Actuarial and Financial Mathematics, Welfengarten 1, 30167 Hannover, Germany*

Abstract

Macroscopic traffic flow models such as the Cell Transmission Model (CTM) are widely used in large-scale traffic simulation; however, discrepancies between macroscopic and microscopic representations persist at unsignalized intersections with conflicting flows. While microscopic simulations predict conflict-induced delays even under low-demand conditions, standard CTM formulations exhibit a systematic macroscopic simulation artifact at unsignalized intersections: as long as flow-dependent capacity constraints are inactive, disturbed movements traverse the intersection at free-flow speed, leading to unrealistically delay-free behavior. This paper addresses this inconsistency by proposing a conflict-aware extension of the CTM (CA-CTM) based on a minimal structural modification of the sending function. Rather than representing conflicts solely through flow-dependent maximal outflow constraints, the effective free-flow speed in selected cells is reduced as a function of opposing demand. This preserves the core structure of the CTM while increasing computational effort only by a constant factor, thereby improving consistency with microsimulation dynamics across different demand regimes. Using controlled simulation-based case studies in an isolated intersection setting and a stylized urban network, we show that standard CTM formulations can be calibrated to align reasonably well with microscopic reference results within individual scenarios but fail to generalize across varying conflict levels. In contrast, the proposed CA-CTM remains sensitive to conflict effects across demand regimes, suggesting that the discrepancies between standard CTM formulations and microscopic reference models under conflicting flows are structural rather than parametric and can be substantially reduced by a minimal intervention.

Keywords: Macroscopic traffic model, Cell transmission model, Conflict-induced flow interactions, Model consistency, Regime behavior

1. Introduction

Macroscopic traffic flow models such as the Cell Transmission Model (CTM) are widely used for large-scale simulation due to their simple update structure and favorable computational properties.

*Corresponding author

Email addresses: `zfeinste@stevens.edu` (Zachary Feinstein),
`justin.plueckebaum@insurance.uni-hannover.de` (Justin Plückebaum),
`stefan.weber@insurance.uni-hannover.de` (Stefan Weber)

Originally developed for freeway applications [1, 2, 3, 4, 5], the CTM has since evolved into a general framework for dynamic network loading and has been extended to increasingly complex network settings. Comprehensive overviews of these developments, with a particular emphasis on urban network applications, are provided by Adacher and Tiriolo [6].

A central challenge in transferring the CTM to urban environments lies in the modeling of intersections. Unlike freeway segments, intersections introduce interaction effects through traffic signals, priority rules, and conflicting movements, which govern how upstream demand is transmitted to downstream supply. In particular, turning movements opposed by oncoming traffic are affected by interaction effects that originate at the node and therefore require additional conditions beyond standard link-based sending and receiving dynamics.

Within the CTM framework, intersections can be represented at different levels of abstraction [7]. Pointwise node models efficiently connect multiple upstream and downstream cells and accommodate general connectivity patterns, but they treat the intersection as an instantaneous transition and therefore do not explicitly represent traversal times within the intersection area [8, 9]. Spatially extended intersection models address this limitation by introducing conditional cells [10] or dedicated turning cells [11]. While this increases modeling fidelity, it also requires additional structural detail and computational effort.

Independent of the chosen intersection representation, a mechanism is required to capture how opposing traffic constrains turning movements and induces conflict-related delays. Existing CTM-based approaches typically represent these interactions through flow-dependent capacity constraints, where the maximal discharge flow of a turning movement is reduced as a function of opposing demand. Such formulations are compatible with both pointwise and spatial intersection models and loosely resemble gap-acceptance behavior [9, 11].

However, when conflict effects are represented solely through such capacity constraints, interaction-induced delays are only reflected once these constraints become binding. As a consequence, under low-demand conditions the disturbed stream may traverse the intersection at free-flow speed, even though microscopic simulations consistently predict non-negligible conflict-induced delays already in this regime. This behavior reveals a discrepancy between macroscopic flow representations and the interaction mechanisms observed in microsimulation.

In practice, this discrepancy is often addressed through scenario-specific parameter calibration, whereby conflict parameters are tuned to reproduce microscopic reference results under a given demand configuration. While such calibration can improve model fit in isolated cases, we show that the observed discrepancy persists systematically across demand regimes, indicating a structural rather than parametric limitation of standard CTM formulations. This behavior is consistent with well-documented issues of parameter identifiability and scenario dependence in macroscopic traffic flow models [12, 13].

In this paper, we propose a structural modification of the CTM that addresses this limitation by incorporating conflict effects directly into the sending function. Instead of representing conflicts solely through reduced discharge capacities, the effective free-flow speed in selected cells is adjusted as a function of opposing demand. This modification introduces a fixed number of additional operations per cell and time step and therefore increases computational effort only by a constant factor. At the same time, it enables the model to capture conflict-induced delays across different demand regimes, including low-density conditions in which standard CTM formulations predict unrealistically unhindered flow. Using controlled simulation-based case studies in an isolated intersection setting and a stylized urban network, we show that standard CTM formulations do not generalize robustly across varying levels of conflict, whereas the proposed conflict-aware formulation retains

sensitivity to conflict effects across demand regimes.

The remainder of the paper is structured as follows. Section 2 reviews the fundamental concepts underlying the CTM and its sending and receiving functions. Section 3 discusses established approaches for modeling conflicting flows at unsignalized intersections within the CTM framework. Section 4 introduces the proposed conflict-aware formulation. Section 5 presents two simulation-based case studies comparing the standard CTM with the proposed formulation in an isolated intersection setting and a stylized urban network. Section 6 concludes the paper.

2. Basics

CTM. The Cell Transmission Model, originally developed by Daganzo [1, 2], is a macroscopic traffic flow model that discretizes roads into a series of cells and updates traffic states over time using principles derived from the Lighthill–Whitham–Richards kinematic wave theory [14, 15]. The traffic conditions are updated in discrete time steps $t = 1, 2, 3, \dots$. Each time step corresponds to a real-world time interval of length ΔT (e.g., 1 second). Each cell i is characterized by a sending function $S_i(\rho_i(t))$ [veh/s] (how much flow it can emit) and a receiving function $R_i(\rho_i(t))$ [veh/s] (how much flow it can accept) that depend on the current density $\rho_i(t)$ [veh/m] at simulation step t . At each time step, the vehicle flow per second from cell i to the next cell $i + 1$ in the time interval $(\Delta T \cdot t, \Delta T \cdot (t + 1))$ is computed as:

$$q_i^{out}(t + 1) = \min\{S_i(\rho_i(t)), R_{i+1}(\rho_{i+1}(t))\}.$$

Based on this inter-cell flow, the density in cell i at the next time step $t + 1$ is updated using the discrete flow conservation equation

$$\rho_i(t + 1) = \rho_i(t) + \frac{\Delta T}{l_i}(q_{i-1}^{out}(t + 1) - q_i^{out}(t + 1)),$$

where l_i is the length of cell i , $q_{i-1}^{out}(t + 1)$ is the inflow from the upstream cell, and $q_i^{out}(t + 1)$ is the outflow to the downstream cell. To ensure numerical stability within the CTM, the Courant–Friedrichs–Lewy condition must be satisfied. This requires that the cell length l_i has to exceed the distance a vehicle can travel at free-flow speed v_i^{free} within a single simulation time step, i.e.,

$$l_i \geq v_i^{free} \cdot \Delta T.$$

In the CTM, traffic streams can split (diverge) or join (merge), requiring special treatment to preserve flow and capacity principles. As our simulation study involves only diverges, we limit the discussion to this case. At a *diverge*, a single upstream cell i splits into two downstream cells ("out₁" and "out₂"). The upstream flow is distributed according to turning fractions $f_{i \rightarrow out_j}$ towards downstream links out _{j} , with $f_{i \rightarrow out_1} + f_{i \rightarrow out_2} = 1$. Based on these turning fractions, the total outflow from the diverging cell is given by

$$q_i^{out}(t + 1) = \min \left\{ S_i(\rho_i(t)), \frac{R_{out_1}(\rho_{out_1}(t))}{f_{i \rightarrow out_1}}, \frac{R_{out_2}(\rho_{out_2}(t))}{f_{i \rightarrow out_2}} \right\}. \quad (2.1)$$

This formulation ensures that the total outflow from the upstream cell does not exceed its sending capacity, that no downstream cell receives more vehicles than it can accommodate, and that the outflow from an upstream cell is accordingly reduced when one or more downstream cells

at the diverge reach capacity, thereby representing spillback and blocking effects at the macroscopic level. Once q_i^{out} is determined, the split flows are computed via:

$$q_{i \rightarrow \text{out}_1}^{out}(t+1) = q_i^{out}(t+1) \cdot f_{i \rightarrow \text{out}_1} \quad \text{and} \quad q_{i \rightarrow \text{out}_2}^{out}(t+1) = q_i^{out}(t+1) \cdot f_{i \rightarrow \text{out}_2}.$$

Sending and Receiving Functions in Standard (Non-Interacting) Road Segments. Most cells in traffic networks, in particular non-conflicting road segments, follow a relatively simple structure, without the complex interactions present at intersections. In principle, the exact shape of the sending and receiving functions is not strictly fixed and can be adapted to reflect different modeling assumptions, as long as they satisfy basic monotonicity and capacity constraints [16]. However, a common standard choice is

$$S(\rho_i(t)) = \min\{v^f \cdot \rho_i(t), q_{\max}\} \quad \text{and} \quad R(\rho_i(t)) = \min\{b \cdot (\rho_{\max} - \rho_i(t)), q_{\max}\},$$

where v^f [m/s] is the free-flow speed, q_{\max} [veh/s] is the maximal possible flow, b [m/s] is the backward wave speed and ρ_{\max} [veh/m] is the jam density.

Cumulative Flow Functions. To analyze delay within the CTM framework, cumulative flow functions are usually used, which describe the sum of all vehicles that have entered or left a cell up to a certain point in time. Under the assumption of constant flows within each simulation step, the cumulative inflow and outflow for cell i can be expressed as follows in the CTM framework:

$$\begin{aligned} cum q_i^{in}(\tilde{t}) &= \sum_{j=1}^{\lfloor \frac{\tilde{t}}{\Delta T} \rfloor} q_i^{in}(j) \cdot \Delta T + \left(\frac{\tilde{t}}{\Delta T} - \left\lfloor \frac{\tilde{t}}{\Delta T} \right\rfloor \right) \cdot q_i^{in} \left(\left\lceil \frac{\tilde{t}}{\Delta T} \right\rceil \right) \cdot \Delta T, \\ cum q_i^{out}(\tilde{t}) &= \sum_{j=1}^{\lfloor \frac{\tilde{t}}{\Delta T} \rfloor} q_i^{out}(j) \cdot \Delta T + \left(\frac{\tilde{t}}{\Delta T} - \left\lfloor \frac{\tilde{t}}{\Delta T} \right\rfloor \right) \cdot q_i^{out} \left(\left\lceil \frac{\tilde{t}}{\Delta T} \right\rceil \right) \cdot \Delta T, \end{aligned}$$

where $\tilde{t} \in \mathbb{R}_+$ denotes the continuous time, and q_i^{in} is defined as the total inflow to cell i , obtained by summing the outflows from all its upstream neighbors.

Travel Time and Delay. Travel times are derived from the area between the cumulative inflow and cumulative outflow curves. Mathematically, the average travel time per vehicle for cell i can be computed, for strictly increasing functions $cum q_i^{in}$ and $cum q_i^{out}$, as

$$\text{Average Travel Time} = \frac{1}{CV_1 - CV_0} \int_{CV_0}^{CV_1} (cum q_i^{out})^{-1}(y) - (cum q_i^{in})^{-1}(y) dy,$$

where CV_0 and CV_1 denote the lower and upper cumulative vehicle numbers considered within the analysis period.

Analogously, delays are derived by comparing the cumulative outflow curve with the corresponding free-flow cumulative outflow curve ${}^{ff} cum q_i^{out}$, i.e., the outflow curve that would be obtained if vehicles traversed the cell without congestion or conflict-related delay. For strictly increasing functions $cum q_i^{out}$ and ${}^{ff} cum q_i^{out}$, the average delay per vehicle can be computed as

$$\text{Average Delay} = \frac{1}{CV_1 - CV_0} \int_{CV_0}^{CV_1} (cum q_i^{out})^{-1}(y) - ({}^{ff} cum q_i^{out})^{-1}(y) dy.$$

Thus, the average travel time per vehicle is given by the sum of the average free-flow travel time and the average delay per vehicle. In Figure 1, these two components are represented by the two shaded areas between the cumulative curves.

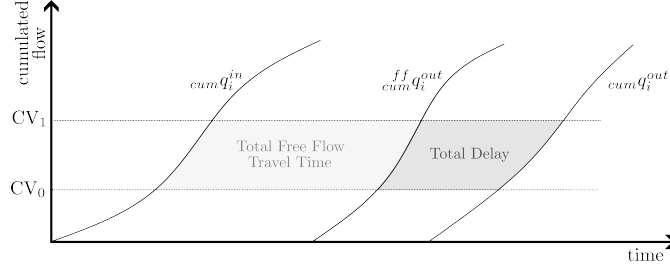


Figure 1: Illustration of travel time and delay based on cumulative flow curves.

3. Representation of Conflicting Flows in the CTM

In this paper, we focus on an idealized unsignalized T-intersection, where a left-turning movement yields to an opposing through flow. Figure 2 illustrates the intersection under consideration. The main part of the intersection is represented by the cell * which consists of three different paths $(in_1, *, out_1)$, $(in_1, *, out_2)$ and $(in_2, *, out_3)$ indicated by different line types. We thus consider a spatially explicit representation of movements within the intersection, as done for example by [17] and [18], rather than simulating the intersection as a point-wise node, as done in the Incremental Node Model by Flötteröd & Rohde [9]. Note that the limitations of existing detailed modeling approaches discussed in Section 5.2 are also present in Flötteröd’s INM. For analytical clarity and isolation of conflict effects, we restrict the analysis to configurations with uncongested downstream links and a single dominant conflict mechanism. Although our focus is on unsignalized intersections, the underlying ideas could in principle be extended to signalized settings that feature conflicting traffic streams. This section examines standard CTM formulations for conflict-impeded left-turning movements at intersections, focusing on common macroscopic adaptations used to approximate interaction effects.

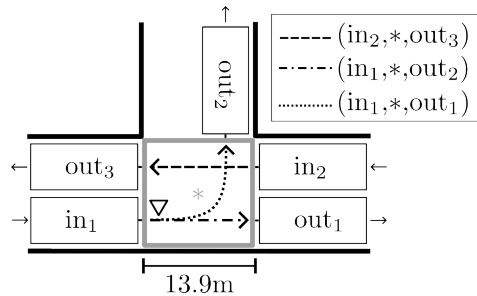


Figure 2: T-Intersection model in the CTM

Speed Adjustment for Turnings. The speed $v_{(in_1, *, out_2)}^f$ for the turning portion of vehicles must be adjusted, as turning maneuvers inherently involve reduced travel speeds due to roadway

geometry and cautious driver behavior. These adjustments are independent of opposing traffic and aim to improve the baseline realism of the model. By modifying the free-flow speed in the sending function relative to regular cells, the model captures reduced throughput associated with turning behavior, without explicitly modeling vehicle-level acceleration or deceleration dynamics.

Interaction of flows. To capture the dynamics of interacting vehicle streams at intersections within the CTM, we focus now on the modeling of left-turning vehicles opposed by through traffic at the T-intersection shown in Figure 2. The outflow from cell in_1 splits into two directed flows, denoted as paths $(in_1, *, out_1)$ and $(in_1, *, out_2)$; thus, in the absence of opposing traffic, the situation corresponds to a standard diverge configuration as described in Equation 2.1. To represent the impediment experienced by left-turning vehicles due to the opposing through movement, a common approach (see, e.g., [11]) is to define a conflict-adjusted function $q^{red}(\cdot)$ that limits the feasible outflow from cell in_1 as a function of the outflow from cell in_2 , representing the opposing stream. Building on Equation 2.1 and omitting time indices for simplicity, the outflow from cell in_1 is then computed as

$$q_{in_1}^{out} = \min \left\{ S_{in_1}(\rho_{in_1}), \frac{R_{(in_1, *, out_1)}(\rho_{(in_1, *, out_1)})}{f_{in_1 \rightarrow out_1}}, \frac{\min\{R_{(in_1, *, out_2)}(\rho_{(in_1, *, out_2)}), q_{(in_1, *, out_2)}^{red}(q_{in_2}^{out})\}}{f_{in_1 \rightarrow out_2}} \right\}, \quad (3.1)$$

where $f_{in_1 \rightarrow out_1}$ and $f_{in_1 \rightarrow out_2}$ with $f_{in_1 \rightarrow out_1} + f_{in_1 \rightarrow out_2} = 1$ denotes the turning fractions and $S_{in_1}(\rho_{in_1}) = \min\{v^f \cdot \rho_{in_1}, q_{max}\}$ is the standard linear sending function. Once $q_{in_1}^{out}$ is determined, the split flows are computed via:

$$q_{(in_1, *, out_1)}^{in} = q_{in_1}^{out} \cdot f_{i \rightarrow out_1} \quad \text{and} \quad q_{(in_1, *, out_2)}^{in} = q_{in_1}^{out} \cdot f_{i \rightarrow out_2}.$$

One frequently used way to define such a conflict-sensitive function is based on an exponentially decaying relationship, as proposed in the German guidelines issued by the Forschungsgesellschaft für Straßen- und Verkehrswesen [19]. This approach has subsequently been adopted in macroscopic intersection modeling, for example by [20]. In this context, the effective outflow for a turning movement can be bounded by:

$$q_{(in_1, *, out_2)}^{red}(q_{in_2}^{out}) = \frac{1}{t_f} \exp \left[-q_{in_2}^{out} \cdot \left(t_g - \frac{t_f}{2} \right) \right]. \quad (3.2)$$

The parameter t_g denotes the critical gap required for a vehicle to safely complete the turning maneuver, while t_f represents the follow-up time between two successive turning vehicles. These values are typically specified based on empirical guidelines or calibrated within simulation-based studies. This function is solely used as an illustrative example; any functional form may be employed as long as it captures the decreasing likelihood of successful turning as the opposing flow increases.

4. A Conflict-Aware Extension of the CTM Sending Function

The standard approach described in the previous section imposes an upper bound on the turning flow by assigning a fixed maximum outflow for each level of opposing traffic. However, when the flow of the turning movement is low and does not reach the threshold at which the upper bound becomes active, standard CTM formulations allow these vehicles to pass at full speed, regardless

of whether opposing traffic would induce delays. This behavior reflects a structural limitation of capacity-based conflict representations. A more refined modeling approach is required to represent conflict effects consistently across different density levels.

Building on the capacity-based conflict representation introduced above, which constrains turning movements through flow-dependent maximum outflow limits, we augment the interaction modeling by additionally adjusting the free-flow speed in selected upstream cells as a function of opposing traffic. Importantly, this refinement preserves the original structure of the CTM and affects only the functional form of the sending functions; receiving functions, conservation equations, and the network loading logic remain unchanged. The speed modification, applied to cells in_1 , $(\text{in}_1, *, \text{out}_1)$, and $(\text{in}_1, *, \text{out}_2)$, captures the reduction in traversal speed caused by increasing opposing flow and thereby provides a more consistent representation of conflict effects than a fixed outflow bound alone. Accordingly, the following expressions are used to compute the flows in the affected cells, where $f_{\text{in}_1 \rightarrow \text{out}_1}$ and $f_{\text{in}_1 \rightarrow \text{out}_2}$ with $f_{\text{in}_1 \rightarrow \text{out}_1} + f_{\text{in}_1 \rightarrow \text{out}_2} = 1$ denote the turning fractions:

$$q_{\text{in}_1}^{\text{out}} = \min \left\{ S_{\text{in}_1}(\rho_{\text{in}_1}, q_{\text{in}_2}^{\text{out}}), \frac{R_{(\text{in}_1, *, \text{out}_1)}(\rho_{(\text{in}_1, *, \text{out}_1)})}{f_{\text{in}_1 \rightarrow \text{out}_1}}, \frac{\min\{R_{(\text{in}_1, *, \text{out}_2)}(\rho_{(\text{in}_1, *, \text{out}_2)}), q_{(\text{in}_1, *, \text{out}_2)}^{\text{red}}(q_{\text{in}_2}^{\text{out}})\}}{f_{\text{in}_1 \rightarrow \text{out}_2}} \right\},$$

$$q_{(\text{in}_1, *, \text{out}_1)}^{\text{out}} = \min\{S_{(\text{in}_1, *, \text{out}_1)}(\rho_{(\text{in}_1, *, \text{out}_1)}, q_{\text{in}_2}^{\text{out}}), R_{\text{out}_1}(\rho_{\text{out}_1})\},$$

$$q_{(\text{in}_1, *, \text{out}_2)}^{\text{out}} = \min\{S_{(\text{in}_1, *, \text{out}_2)}(\rho_{(\text{in}_1, *, \text{out}_2)}, q_{\text{in}_2}^{\text{out}}), R_{\text{out}_2}(\rho_{\text{out}_2})\},$$

where the only modification introduced by our approach is reflected in the sending functions, whose effective free-flow speed is adjusted based on the level of opposing traffic:

$$S_{\text{in}_1}(\rho_{\text{in}_1}, q_{\text{in}_2}^{\text{out}}) = \min\{v_{\text{in}_1}^f(q_{\text{in}_2}^{\text{out}}) \cdot \rho_{\text{in}_1}, q_{\text{max}}\},$$

$$S_{(\text{in}_1, *, \text{out}_1)}(\rho_{(\text{in}_1, *, \text{out}_1)}, q_{\text{in}_2}^{\text{out}}) = \min\{v_{(\text{in}_1, *, \text{out}_1)}^f(q_{\text{in}_2}^{\text{out}}) \cdot \rho_{(\text{in}_1, *, \text{out}_1)}, q_{\text{max}}\},$$

$$S_{(\text{in}_1, *, \text{out}_2)}(\rho_{(\text{in}_1, *, \text{out}_2)}, q_{\text{in}_2}^{\text{out}}) = \min\{v_{(\text{in}_1, *, \text{out}_2)}^f(q_{\text{in}_2}^{\text{out}}) \cdot \rho_{(\text{in}_1, *, \text{out}_2)}, q_{\text{max}}\}.$$

To guarantee that the modification behaves appropriately under varying levels of opposing traffic, the effective free-flow speeds must satisfy:

$$v_k^f(0) = v_k^f, \quad \frac{d}{dq_{\text{in}_2}^{\text{out}}} v_k^f(q_{\text{in}_2}^{\text{out}}) \leq 0, \quad v_k^f(q_{\text{in}_2}^{\text{out}}) \geq 0, \quad k \in \{\text{in}_1, (\text{in}_1, *, \text{out}_1), (\text{in}_1, *, \text{out}_2)\},$$

which ensures that the effective free-flow speed equals the standard free-flow speed in the absence of opposing traffic, is non-increasing in the opposing flow, and never becomes negative. Here, $v_k^f(q_{\text{in}_2}^{\text{out}})$ denotes the conflict-dependent effective free-flow speed in cell k , whereas v_k^f without argument denotes the corresponding baseline free-flow speed in the absence of opposing traffic.

A flexible specification that also permits a threshold-like onset of speed reduction is

$$v_k^f(q_{\text{in}_2}^{\text{out}}) = \min\left\{v_k^f, a_k + b_k \exp(c_k \cdot q_{\text{in}_2}^{\text{out}})\right\},$$

with $a_k \geq 0$, $b_k > 0$, $c_k < 0$, and $a_k + b_k \geq v_k^f$. This form allows for an initial plateau at the standard free-flow speed, so that low levels of opposing flow do not necessarily induce an immediate speed reduction. Once the opposing flow exceeds a certain level, the effective free-flow speed decreases

monotonically and approaches the nonnegative lower bound a_k for large opposing flows. In practice, the choice of functional form should depend on the expected interaction pattern and the available calibration data. If opposing flow is expected to affect the traversing stream immediately, a smooth monotone decay may be appropriate. If, however, small opposing flows are expected to have little effect and the reduction sets in only beyond a certain conflict level, the minimum-based form above provides a natural specification. The corresponding parameters can be calibrated jointly with the other model parameters by fitting simulated cumulative flows to reference data across scenarios with different levels of opposing traffic.

Figure 3 illustrates the functions used to compute the flow under a constant opposing flow $q_{in_2}^{out} > 0$ and in a simplified setting where $f_{in_1 \rightarrow out_2} = 1$, which is chosen to clearly demonstrate how the modified conflict-aware sending functions behave in comparison to the standard formulation. Unlike standard formulations, the sending flow depends not only on downstream supply but also on opposing traffic. As shown in both Figures 3a and 3b, whenever opposing traffic is present, the sending function is modified across all density regimes, thereby altering the flow–density relationship even when capacity constraints are not active.

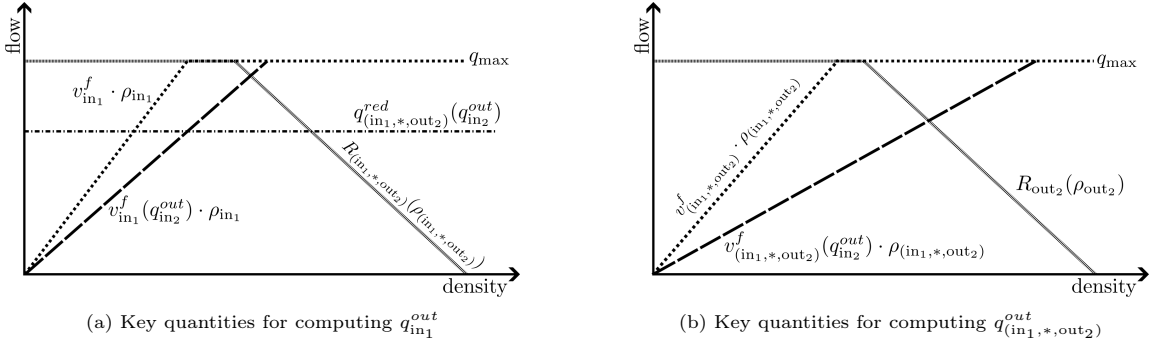


Figure 3: Illustration of the standard and conflict-aware CTM flow constraints determining the outflow, including sending, receiving, and conflict-related bounds, for a fixed value of $q_{in_2}^{out} > 0$.

To the best of our knowledge, incorporating conflict effects through modifications of cell-level sending speeds as a function of opposing traffic, rather than exclusively through capacity constraints, has not yet been formally analyzed within the CTM framework. This speed adjustment introduces a fundamental difference relative to standard CTM formulations, in which vehicles traverse the intersection at free-flow speed whenever capacity constraints are inactive, regardless of opposing traffic. As a result, conflict-induced delays are not reflected in the low-density regime, leading to an internally inconsistent macroscopic representation. By dynamically reducing effective sending speeds as a function of opposing flow, the proposed conflict-aware modification allows interaction effects to influence travel times even when explicit maximal outflow constraints are inactive. This yields a more consistent representation of conflict-induced delays across demand regimes within the macroscopic framework.

Importantly, these modeling benefits are achieved without increasing the asymptotic computational complexity of the cell update. For each affected cell, the additional effort consists of evaluating a single scalar function of the opposing flow per time step, so that the per-cell update complexity remains $O(1)$.

The proposed formulation is intentionally restricted to configurations in which a single traffic stream is subject to a single dominant conflict mechanism. This includes both shared-lane settings and exclusive turning lanes, which can be represented as special cases through appropriate turning fractions. While the following case studies consider an isolated unsignalized T-intersection and a stylized urban network with this type of conflict structure, the underlying idea is not restricted to these specific settings. More complex unsignalized intersections may involve multiple simultaneous conflicts affecting several turning or crossing movements, which would require movement-specific conflict-dependent sending adjustments and a corresponding generalization of the node model. Similar extensions would arise for more general merge and diverge structures, pedestrian interference, or permissive turning phases at signalized intersections. Such multi-conflict formulations are beyond the scope of the present paper, as they would introduce additional interaction variables and calibration choices that increase model complexity without changing the underlying conflict-aware logic. Focusing on a single dominant conflict therefore allows the core contribution to be presented and evaluated more clearly.

5. Case Studies

This section presents two case studies to evaluate the proposed conflict-aware CTM in complementary settings. We first analyze an isolated single-intersection setup to illustrate the calibration of the continuous conflict-dependent speed functions, and then consider a stylized urban network to investigate the behavior of the competing formulations under interacting traffic conditions. In both case studies, the CTM variants are compared against data generated with Aimsun 23.0.0, which is not treated as empirical ground truth, but rather as a consistent and well-established microsimulation benchmark under identical demand and control conditions. Throughout, detector values are recorded at one-second intervals to ensure consistent and detailed data collection.

5.1. Single-Intersection Case Study

We first consider an isolated single-intersection setup, in which the competing CTM formulations are calibrated against Aimsun data over a range of opposing-flow conditions and then compared in terms of the resulting travel times.

5.1.1. Simulation Setup and CTM Model Variants

We consider the isolated unsignalized T-intersection shown in Figure 2. In the simulations, each incoming and outgoing road is modeled over a length of 208.5m, corresponding to 15 CTM cells per link. The downstream boundaries are modeled as unimpeded exits, so that vehicles leaving the considered area are not subject to any further restrictions.

The opposing stream consists exclusively of through-moving vehicles. The conflict-affected stream uses a single shared lane and is composed of 60% left-turning and 40% through-moving vehicles. For the conflict-affected approach, we consider two demand levels, namely 0.15 and 0.45 veh/s. For the opposing approach, the inflow values $\{0, 0.12, 0.16, 0.20, 0.24, 0.28, 0.32, 0.36, 0.40\}$ veh/s are used for parameter identification, whereas the intermediate values $\{0.14, 0.18, 0.22, 0.26, 0.30, 0.34, 0.38\}$ veh/s serve as an additional consistency check for the fitted models.

For each scenario, a constant entry demand is applied for 90s, after which no further vehicles are admitted to the network. Each scenario is simulated for 200s in total to ensure that all vehicles

have left the modeled area. Each scenario is simulated 50 times in Aimsun. The resulting flows at the boundaries of the modeled area, i.e., 208.5 m upstream and downstream of the intersection, are recorded and used as the reference for parameter identification and for the comparison of the CTM variants.

Common CTM Settings. For both case studies, all standard cells in the considered CTM variants follow linear sending and receiving functions of the form

$$S(\rho_i(t)) = \min\{v^f \cdot \rho_i(t), q_{\max}\}, \quad R(\rho_i(t)) = \min\{b \cdot (\rho_{\max} - \rho_i(t)), q_{\max}\},$$

where $v^f = 13.9$ m/s denotes the free-flow speed, $b = 4.214$ m/s the backward wave speed, $\rho_{\max} = 0.2$ veh/m the jam density, and $q_{\max} = 0.629$ veh/s the maximum flow. These parameters were determined from an Aimsun highway simulation with an allowed speed of 50 km/h. For cells representing left-turning traffic at intersections, a reduced free-flow coefficient of 7 m/s is used to reflect the lower turning speed. In addition, for the cell immediately upstream of the diverge, a reduced maximum flow of $q_{\max} = 0.54$ veh/s is used to represent the lower effective discharge capacity caused by the turning maneuver and the associated node interaction. In all CTM simulations, the time step is set to $\Delta T = 1$ s and the standard cell length to 13.9 m.

CTM and CA-CTM. The single-intersection setup considered here corresponds exactly to the setting described in Sections 3 and 4, and we therefore use the same notation for the incoming and outgoing movements. For the reduction of the admissible outflow caused by opposing traffic, we adopt the functional form

$$q_{(\text{in}_1, *, \text{out}_2)}^{\text{red}}(q_{\text{in}_2}^{\text{out}}) = a_q + b_q \exp(c_q \cdot q_{\text{in}_2}^{\text{out}}), \quad (5.1)$$

with $a_q \geq 0$, $b_q > 0$ and $c_q < 0$. Accordingly, the standard CTM requires the identification of the three parameters entering this conflict-related outflow function.

For the CA-CTM, the same conflict-dependent outflow function is used, but in addition the effective free-flow speeds in the affected cells

$$k \in \{\text{in}_1, (\text{in}_1, *, \text{out}_1), (\text{in}_1, *, \text{out}_2)\}$$

are modeled as

$$v_k^f(q_{\text{in}_2}^{\text{out}}) = \min\left\{v_k^f, a_k + b_k \exp(c_k \cdot q_{\text{in}_2}^{\text{out}})\right\},$$

with $a_k \geq 0$, $b_k > 0$, $c_k < 0$, and $a_k + b_k \geq v_k^f$.

The inflows used in the CTM variants are obtained from the average inflow profiles over the 50 Aimsun replications and are aggregated to piecewise-constant values over 5s intervals, since the microscopic inflows exhibit strong short-term fluctuations that are not represented at the macroscopic level. Likewise, the turning percentages used in the CTM are taken from the averages over the same 50 Aimsun runs.

5.1.2. Parameter Identification and Model Evaluation

In the following case studies, the term *calibration* refers to parameter identification under controlled simulation conditions using the microscopic reference model Aimsun. It is employed as a diagnostic

tool to examine regime-dependent structural behavior of the different CTM formulations, rather than as an empirical calibration to field data.

Parameter estimation in macroscopic traffic models such as the CTM is often performed using loop detector data, especially vehicle counts [21]. A key methodological refinement was proposed by Punzo and Montanino [22], who argue that cumulative variables, such as cumulative flow curves, should be preferred over instantaneous variables like pointwise flow or speed. One major advantage of cumulative flows is that they preserve the temporal structure of deviations, thereby smoothing noise and highlighting systematic discrepancies.

For each scenario in the calibration set, the mean squared errors of the cumulative outflow curves at the downstream boundary of the modeled area for left-turning and through-moving vehicles are combined using weights given by the corresponding turning fractions. As the microscopic reference, we use the corresponding cumulative outflow curves averaged over the 50 Aimsun replications. The model parameters are then identified by minimizing the resulting weighted mean squared error over the calibration data. The resulting minimized objective values are 0.238 for the CTM and 0.049 for the CA-CTM, indicating a substantially better fit of the conflict-aware formulation to the calibration data. The corresponding calibrated parameter values are reported in Table 1.

Model	Parameter	Calibrated value
CTM	a_q	0.0109
	b_q	0.3125
	c_q	-5.0450
CA-CTM	a_q	0.0000
	b_q	0.4051
	c_q	-4.6964
	a_{in_1}	1.008
	b_{in_1}	13.7000
	c_{in_1}	-17.5532
	$a_{(in_1,*,out_1)}$	0.4778
	$b_{(in_1,*,out_1)}$	6.7003
	$c_{(in_1,*,out_1)}$	-7.0006
	$a_{(in_1,*,out_2)}$	4.8884
	$b_{(in_1,*,out_2)}$	47.7904
	$c_{(in_1,*,out_2)}$	-21.1763

Table 1: Calibrated parameter values for the CTM and CA-CTM in the single-intersection case study.

Figure 4 compares the average travel times predicted by the standard CTM and the CA-CTM with the Aimsun reference for left-turning and through-moving vehicles on the conflict-affected approach. For the Aimsun reference, the error bars show an approximate 95% confidence interval for the mean travel time, computed as the sample mean over the 50 replications, plus and minus two standard errors.

For the high-demand scenario, the standard CTM reproduces the observed travel times reasonably well over most opposing-flow levels. In this regime, the conflict-dependent outflow bound is frequently active and can therefore capture a substantial part of the delay caused by opposing traffic. As a result, the corresponding CTM travel times lie within or close to the Aimsun confidence intervals. The limitations of the standard CTM become apparent in the low-demand scenario. For opposing inflows up to approximately 0.26 veh/s, the predicted travel times remain nearly un-

changed, because the conflict-related outflow bound is not yet active. Hence, the model does not reflect the delay effects that are already induced by opposing traffic in the microscopic reference. Once the bound becomes active, the CTM travel times start to rise with increasing opposing flow. For through-moving vehicles, this eventually leads to values that lie inside the Aimsun confidence intervals, whereas for left-turning vehicles the standard CTM remains systematically below the reference throughout the considered range. Even so, the discrepancies remain non-negligible: the predicted average travel times deviate by up to about 10s from the 95% confidence interval for left-turning vehicles and by up to about 5s for through-moving vehicles.

By contrast, the CA-CTM captures the increase in travel times more consistently across both demand levels and both movement types. In particular, its average travel times lie within or close to the Aimsun confidence intervals for nearly all considered opposing-flow levels. Moreover, the predicted travel times increase monotonically with opposing flow, consistent with the expectation that stronger opposing traffic reduces usable gaps and thereby slows movement through the conflict area. The displayed opposing inflow levels include both the values used for parameter identification and intermediate values considered separately for an additional plausibility check. The good agreement across the full range of inflow levels suggests that the fitted model captures the underlying trend reasonably well. Overall, these results indicate that the additional conflict-dependent speed reduction provides a more consistent macroscopic representation of travel-time effects, especially in regimes where opposing traffic already induces delay although the capacity-related outflow bound is not yet binding.

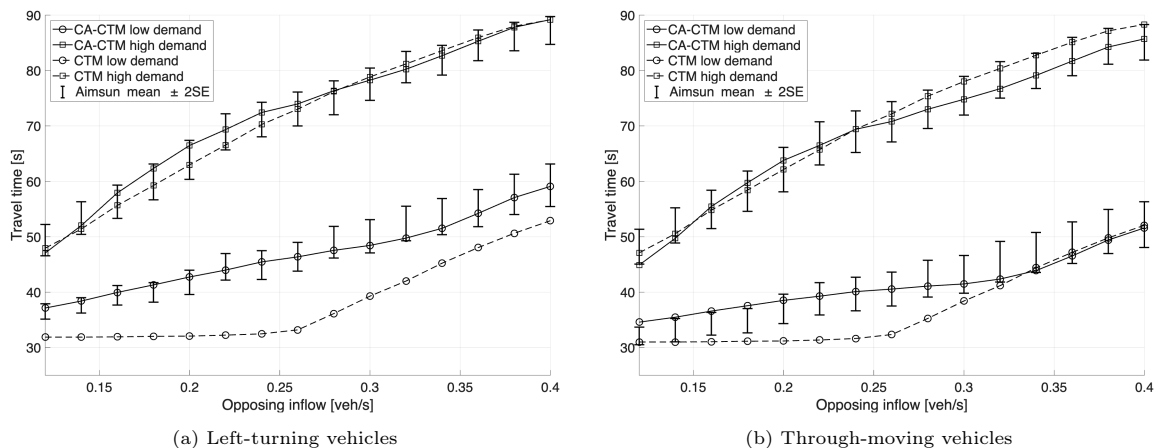


Figure 4: Average travel times as a function of the opposing inflow. The curves show the predictions of the standard CTM and the CA-CTM for low- and high-demand regimes, while the error bars indicate the Aimsun mean travel time ± 2 standard errors over 50 replications.

5.2. Stylized Urban Network Case Study

While the preceding single-intersection study focuses on calibration and controlled comparison in an isolated setting, the present case study considers a stylized urban network to demonstrate that the conflict situations targeted by the proposed formulation arise naturally at the network level and can materially affect macroscopic traffic dynamics.

5.2.1. Network Setup and CTM Model Variants

To evaluate the structural behavior of the competing macroscopic formulations under controlled variation in conflict intensity, we consider the stylized network in Figure 5. The network consists of three intersections connected by single-lane standard road segments with an allowed speed of 50km/h. The possible vehicle routes are also illustrated in the figure, highlighting the central role of the unsignalized intersection I2 for interaction modeling. This is precisely the location at which we evaluate the proposed extension to the standard CTM. Signalized locations are marked with red lines, indicating that the inflows from I1 and I3 into the direction of I2 are controlled by a traffic signal. Both signals switch to green simultaneously, allowing vehicles to enter the network. Each green phase lasts 50 seconds, followed by a red phase that continues until all vehicles have exited the network. Because of the synchronized signal timings, the interacting traffic streams reach the central intersection I2 nearly at the same time. In this case study, we focus on a single green phase, assuming that during the preceding red phase, approximately 23 to 25 vehicles have accumulated at both signalized intersections. The detector locations are shown in Figure 5; both detectors measure the flow originating from I1, which splits at I2 into left-turning and through movements that share a single lane and are therefore jointly affected by opposing traffic.

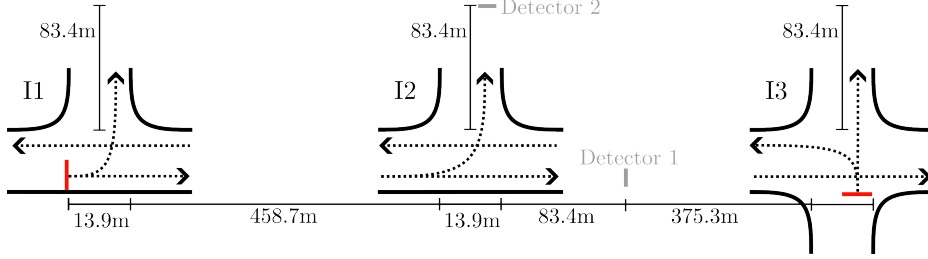


Figure 5: Network layout of the case study used to isolate conflict-induced interactions at intersection I2 while keeping all other network elements fixed.

Demand Scenarios. We investigate three scenarios that differ in the turning ratios at intersection I1, while the ratios at intersections I2 and I3 remain constant (see Table 2). Scenario 1 results in a low flow from intersection I1 to I2, i.e., a low volume of the traffic stream that is subject to obstruction at I2. Scenario 2 corresponds to a medium level of this affected flow, while Scenario 3 results in a high volume. The obstructing flow at I2 remains unchanged across all scenarios due to constant turning ratios at intersection I3. Each scenario is simulated 100 times in Aimsun, and the average results are used as a reference for comparison. The actual turning fractions were extracted from these averaged simulations and then used as input parameters for the CTM-based simulations. The scenario design isolates variation in the conflict-affected stream, while keeping all other network and control elements fixed, thereby enabling an independent examination of the effects of conflict representation.

CTM. As in the previous case study, we adopt the same general CTM and CA-CTM formulations introduced earlier and retain the same baseline model parameters. In the present network setting, however, the additional constraint for obstructed left-turning vehicles can be simplified in a natural way. The opposing flow q_{in2}^{out} , which generates the obstruction for the left-turning vehicles at intersection I2, is shown in Figure 6 and exhibits nearly the same pattern across all scenarios. As the figure illustrates, this opposing flow is almost always either zero or approximately constant

Scenario	I1 - left	I1 - straight	I2 - left	I2 - straight	I3 - left	I3 - straight
1	0.75	0.25	0.4	0.6	0.5	0.5
2	0.5	0.5	0.4	0.6	0.5	0.5
3	0.25	0.75	0.4	0.6	0.5	0.5

Table 2: Overview of the turning fractions of all scenarios.

in the CTM. This reflects CTM behavior under signal control, where the upstream signal causes the outflow to switch from zero to the maximal discharge flow during green phases until the queue is discharged. As a result, the opposing stream reaches the conflict area in platoon-like arrivals, leading to alternating periods of zero flow and approximately constant positive flow rather than continuously varying inflow. Under these conditions, it is reasonable to replace the general functional relationship $q^{\text{red}}(q_{\text{in}_2}^{\text{out}})$ by the simplified representation

$$q^{\text{red}}(q_{\text{in}_2}^{\text{out}}) = \begin{cases} q_{\text{max}}, & q_{\text{in}_2}^{\text{out}} = 0, \\ q^{CS}, & q_{\text{in}_2}^{\text{out}} > 0, \end{cases}$$

where $q^{CS} < q_{\text{max}}$ is a constant representing the effective capacity under obstruction. Consequently, the conflict constraint is either inactive (when no opposing traffic is present) or limits the flow to a fixed value, so that only the single parameter q^{CS} must be estimated.

This binary specification is specific to the present case study. In the first case study, a more general continuous non-increasing formulation was already used and calibrated; the same formulation can likewise be applied here whenever the opposing flow varies more continuously over time.

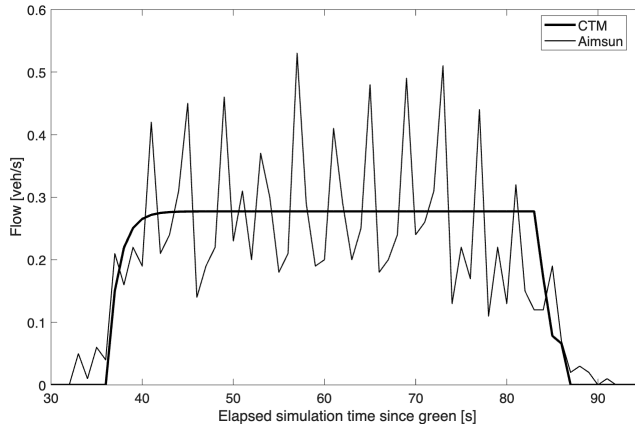


Figure 6: Comparison of microscopic and macroscopic flows of the opposing traffic for Scenario 1. The Aimsun curve is averaged over 100 runs. The corresponding flow profiles for Scenarios 2 and 3 are very similar.

CA-CTM. Analogously to the simplified CTM conflict constraint discussed above, the conflict-dependent free-flow speed functions in the CA-CTM can be simplified in the present case study

to

$$v_k(q_{in_2}^{out}) = \begin{cases} v_k^f, & q_{in_2}^{out} = 0, \\ v_k^{CS}, & q_{in_2}^{out} > 0, \end{cases}$$

where $k \in \{in_1, (in_1, *, out_1), (in_1, *, out_2)\}$. In addition to the previously introduced parameter q^{CS} , which specifies the conflict-induced capacity for the left-turning movement, the CA-CTM therefore requires three additional parameters v_k^{CS} to be calibrated. These parameters define the effective speeds under opposing traffic for the cells inside the intersection as well as for the diverging cell.

Signal Modeling. In the Cell Transmission Model, adjustments are necessary when implementing traffic signals. Due to the lack of acceleration dynamics in the CTM, flow increases immediately during a green phase, whereas in reality, vehicles do not start moving instantaneously but the out-flow builds up gradually. One of the earliest modeling approaches by Webster [23] compensates this by introducing a start-up lost time to capture initial delays. An alternative approach modifies the sending function by introducing a linearly decreasing profile that reduces the admissible flow under oversaturated conditions [24]. In our study, we incorporate a fixed lost time of 2 seconds to better approximate the transient discharge behavior observed in microscopic simulation at signals.

5.2.2. Parameter Identification and Model Evaluation

We calibrate the models by minimizing a weighted sum of the mean squared errors between the cumulative flow curves produced by the respective CTM variant and the corresponding Aimsun average curves at Detectors 1 and 2. The detector-specific weights are chosen proportional to the corresponding turning fractions, so that movements with larger traffic volumes contribute more strongly to the objective function. In joint calibrations involving two scenarios, both scenarios enter the objective function with equal weight.

However, while cumulative flow curves are well suited for calibration, they are often less intuitive to interpret directly. To facilitate interpretation, we therefore consider average delay as a derived performance indicator. Since it is computed from the cumulative flow curves, it provides a more compact and interpretable summary of model performance. To obtain a delay-free reference for delay computation, we perform 100 additional Aimsun simulations per demand scenario with the flow from intersection I3 disabled. This ensures unhindered flow from I1 through I2 and allows baseline free-flow travel times to Detector 1 and Detector 2 to be estimated as averages over these runs. Reported delays are measured relative to these baseline travel times.

For validation, each calibrated model is evaluated on the scenarios that were not used for parameter estimation. Using the same performance measure, this out-of-sample evaluation assesses the model's ability to generalize beyond the calibration scenarios.

To illustrate the magnitude of the scenario-dependent differences observed in the microsimulation reference, Table 3 reports the mean delay across the Aimsun replications, together with the corresponding standard deviation and approximate 95% confidence intervals for the mean based on the standard error. The delay exhibits substantial run-to-run variability, which is expected in microscopic simulations due to stochastic vehicle arrivals, turning fractions, and gap-acceptance interactions at the conflict point. However, because the results are averaged over 100 runs, the standard error of the mean is much smaller, allowing clear differences in mean delay across scenarios to be identified.

Detector	Mean delay [s/veh] with 95% CI for the mean			SD of delay [s/veh]		
	Scenario 1	Scenario 2	Scenario 3	Scenario 1	Scenario 2	Scenario 3
1	4.41 ± 1.55	11.10 ± 1.80	16.16 ± 2.17	7.75	9.01	10.85
2	9.65 ± 1.82	13.97 ± 1.80	18.23 ± 2.06	8.77	9.01	10.29

Table 3: Mean delay and variability across scenarios based on 100 Aimsun replications.

5.2.3. Single-Scenario Calibration

Calibrating the parameter q^{CS} for the CTM to Scenario 1, 2, or 3 yields 0.0450, 0.0674, and 0.0769 veh/s, respectively. For the specified left-turning fraction of approximately 0.4 at intersection I2, the resulting effective approach capacities under opposing traffic are 405, 606.6, and 692.1 veh/h. These values may appear low at first glance; however, they do not represent the nominal capacity of the approach, but the conflict-constrained discharge rate under sustained opposing flow. Moreover, q^{CS} is only active while opposing traffic is present. Once the opposing flow drops to zero, the constraint is removed and the approach discharges at the regular CTM capacity defined by the sending and receiving functions. The resulting delay values for the CTM and the CA-CTM are reported in Table 4. As the table shows, the in-sample performance of the CTM is satisfactory, indicating that it reproduces the traffic dynamics of the calibration scenario reasonably well. This aligns with findings from previous studies - such as the work by Flötteröd and Rohde [9] - where models calibrated and validated within a single scenario are able to closely replicate microscopic simulation results. However, out-of-sample performance deteriorates considerably: models calibrated to a fixed flow level tend to underestimate delays under lower demand and overestimate them under higher demand. In Scenario 1, the CTM yields identical delay predictions when calibrated to Scenarios 2 or 3. Under these low-demand conditions, the conflict-related capacity constraint remains inactive, so vehicles traverse the intersection at the standard free-flow speed regardless of the calibrated conflict parameter. As a result, the cumulative flow curves, and hence the delay values, are unchanged across these calibrations. The remaining delay observed in Scenario 1 is therefore not caused by active conflict effects, but by a small systematic difference between the unconstrained CTM and the unhindered microsimulation baseline. This leads to baseline delays of about 2.56s for through-moving vehicles and 0.9s for left-turning vehicles. Conversely, when the model is calibrated to Scenario 1, the in-sample fit is satisfactory, but delays in the higher-demand scenarios are clearly overestimated. This effect becomes more pronounced as demand increases and is particularly strong in Scenario 3, where the predicted delays substantially exceed the microscopic reference. Overall, these results show that CTM parameterizations in which conflict effects are represented solely through opposing-flow-dependent maximal outflow constraints do not generalize robustly across scenarios with different levels of conflict.

The corresponding results for the CA-CTM indicate that the additional speed-based mechanism alleviates this limitation, although regime-dependent differences remain when calibration is based on only a single scenario. The calibrated CA-CTM parameters are reported in Table 5. As expected, the in-sample results improve relative to the standard CTM, since the CA-CTM introduces additional parameters through the conflict-dependent speed functions. A notable feature is that the predicted delays are now consistently higher for left-turning vehicles than for through-moving vehicles, which is plausible because left-turners are exposed more directly to the conflict and therefore experience stronger interaction effects; this pattern is also visible in the Aimsun reference data. At the same time, calibration to only one scenario still leads to noticeable regime-dependent differences. If the CA-CTM is calibrated to Scenario 1, the delays in Scenarios 2 and 3 are still substantially

overestimated, because the fitted conflict representation implies unrealistically strong obstruction once the capacity constraint becomes active. By contrast, when the model is calibrated to Scenario 2 or 3, the additional speed parameters reduce the effective speeds below their baseline values under opposing traffic, so that delays also increase in Scenario 1, even though the capacity constraint itself is not binding there. Although the resulting delays do not fully align with the Aimsun reference in all cases, they are substantially closer than the corresponding CTM predictions. This illustrates that the speed-based extension allows conflict effects to influence low-demand conditions as well, in contrast to the standard CTM.

Calibration to Scenario	Detector	CA-CTM: Average delay [s/veh]			CTM: Average delay [s/veh]			
		Scenario 1	Scenario 2	Scenario 3	Scenario 1	Scenario 2	Scenario 3	
1	1	4.98	18.06	25.09	6.75	19.72	27.20	
	2	10.65	20.73	27.25	5.10	18.92	27.06	
2	1	3.58	10.98	18.48	2.56	11.95	20.01	
	2	8.65	14.58	21.50	0.90	11.16	19.87	
3	1	3.55	9.08	16.67	2.56	8.99	17.21	
	2	7.35	12.19	19.35	0.90	8.20	17.08	
					Aimsun	4.41 ± 1.55	11.10 ± 1.80	16.16 ± 2.17
						9.65 ± 1.82	13.97 ± 1.80	18.23 ± 2.06

Table 4: Average delays for CA-CTM and CTM calibrated to one scenario. Bold values indicate in-sample scenarios. The target values from Aimsun, which should be matched, are listed below the table.

Calibration Scenario	$v_{in_1}^{CS}$	$v_{(in_1,*,out_1)}^{CS}$	$v_{(in_1,*,out_2)}^{CS}$	q^{CS}
1	12.53	13.90	1.17	0.0483
2	6.86	13.85	1.35	0.0707
3	6.98	13.88	1.64	0.0772

Table 5: Calibrated parameters of the CA-CTM.

5.2.4. Double-Scenario Calibration

Calibrating the parameter q^{CS} for the CTM to Scenarios 1 and 2, 1 and 3, or 2 and 3 yields values of 0.0675, 0.0770 and 0.0727 veh/s, respectively, when opposing traffic is present. The results of the parameter calibration of the CA-CTM are shown in Table 7. The resulting average delays are summarized in Table 6.

In Scenario 1, the delay predicted by the CTM is identical regardless of which pair of scenarios is used for calibration. This is again because, under these low-demand conditions, the conflict-related capacity constraint does not become active, so that vehicles traverse the intersection at the standard free-flow speed. As a result, the cumulative flow curves, and therefore also the resulting delays, are identical to those obtained in the single-scenario calibration based on Scenario 2 or 3. Compared to single-scenario calibration, double-scenario calibration for the CTM leads to a noticeable degradation in in-sample performance. This behavior arises from the structural limitations of the standard CTM formulation. For a given level of opposing flow, the CTM contains only a single parameter that governs the turning movement, namely the maximum inflow into the intersection for the left-

turning vehicles. When calibrating to two different demand scenarios, this single parameter cannot simultaneously reproduce both conditions: improving the fit for one scenario necessarily worsens the fit for the other, or forces the calibration to settle at a compromise that represents neither scenario well. As a result, in-sample performance deteriorates under double-scenario calibration.

In contrast, the CA-CTM generally yields closer agreement with the Aimsun-generated delay values across the considered calibration–evaluation combinations. The only clear exception occurs when the model is calibrated to Scenarios 1 and 2 and then evaluated out-of-sample on Scenario 3, where the predicted delays are too high. In all other cases, the predicted delays lie within the approximate 95% confidence intervals around the Aimsun mean values. This suggests that the CA-CTM not only captures scenario-specific behavior more accurately, but also generalizes more reliably across varying traffic conditions. Compared with the in-sample results of the CTM calibrated to a single scenario, the two-scenario calibration of the CA-CTM still yields a comparable level of in-sample accuracy and in some cases even closer agreement with the Aimsun mean delay values. Overall, these results indicate that the CA-CTM can interpolate more robustly across different demand levels. Although they do not point to a single optimal choice of calibration scenarios, they suggest that including the high-demand scenario is beneficial, because it constrains the model in the regime where conflict effects act on many vehicles and thus helps avoid unrealistically large delays being propagated through the system. A systematic investigation of which demand levels are most informative for calibration remains an interesting question for future research.

The two case studies confirm that the limitations of standard CTM conflict modeling are structural rather than merely parametric. Both in the isolated intersection setting and in the stylized urban network, the standard formulation can be calibrated to match individual scenarios reasonably well, but it fails to transfer consistently across demand regimes. As a result, applying parameters identified under one operating condition to another can lead to systematic distortions in simulated cumulative flows and derived performance measures such as travel times and delays. By introducing conflict-dependent speeds into the sending dynamics, the proposed CA-CTM reduces this regime dependence, provides a more consistent macroscopic representation of conflict effects, and yields more reliable simulation results across different demand conditions.

Calibration to Scenario	Detector	CA-CTM: Average delay [s/veh]			CTM: Average delay [s/veh]		
		Scenario 1	Scenario 2	Scenario 3	Scenario 1	Scenario 2	Scenario 3
1, 2	1	4.47	11.03	18.41	2.56	11.93	19.99
	2	9.92	14.97	21.69	0.90	11.14	19.85
1, 3	1	4.82	9.35	16.68	2.56	8.98	17.21
	2	9.30	13.03	19.80	0.90	11.14	19.85
2, 3	1	5.06	10.06	17.33	2.56	10.26	18.43
	2	9.18	13.38	20.18	0.90	9.47	18.29
	1			Aimsun	4.41 ± 1.55	11.10 ± 1.80	16.16 ± 2.17
	2				9.65 ± 1.82	13.97 ± 1.80	18.23 ± 2.06

Table 6: Average delays for CA-CTM and CTM calibrated to two scenarios. Bold values indicate in-sample scenarios. The target values from Aimsun, which should be matched, are listed below the table.

Calibration Scenarios	$v_{in_1}^{CS}$	$v_{(in_1,*,out_1)}^{CS}$	$v_{(in_1,*,out_2)}^{CS}$	q^{CS}
1, 2	4.76	13.85	1.26	0.0715
1, 3	4.25	13.85	1.44	0.0782
2, 3	3.96	13.77	1.51	0.0759

Table 7: Calibrated parameters of the CA-CTM.

6. Conclusion

This paper proposed a conflict-aware extension of the Cell Transmission Model that addresses a structural limitation in the macroscopic representation of unsignalized intersections with opposing flows. By incorporating conflict effects directly into the sending function through flow speeds that depend on opposing traffic, the model allows interaction-induced delays to influence traffic dynamics even in low-demand regimes, where standard CTM formulations remain insensitive.

Controlled simulation-based case studies showed that conventional capacity-based conflict representations exhibit regime-dependent behavior: while they can be calibrated to provide a good fit within individual demand scenarios, they fail to generalize when the demand of the conflict-affected stream varies under a fixed level of opposing traffic. In contrast, the proposed formulation maintains sensitivity to opposing traffic across demand regimes. The modification preserves the core structure and computational properties of the CTM, increasing per-cell update effort only by a constant factor.

While the analysis focused on a stylized intersection with a single dominant conflict, the results indicate that conflict-aware sending dynamics can improve the robustness of macroscopic traffic flow models across different demand regimes. The present study relies on validation against a controlled microsimulation reference rather than field observations, which is appropriate for isolating structural differences between model formulations under comparable conditions. At the same time, calibration and validation using real-world traffic data remain important directions for future research in order to further assess the empirical validity and practical applicability of the proposed approach. Extending the model to more complex intersection configurations and interaction patterns likewise represents a relevant avenue for future work.

Acknowledgments

The authors used AI-assisted tools (ChatGPT) to improve wording and grammar. All scientific content, interpretations, and conclusions were fully created, verified, and approved by the authors.

The authors gratefully acknowledge Aimsun for providing a research software license that supported this study.

Conflicts of Interest

The authors declare that there is no conflict of interest regarding the publication of this article.

Data availability

The data that support the findings of this study were obtained under a research license from Aimsun and are therefore subject to restrictions. The data are not publicly available, but may be obtained from the corresponding author upon request and with permission from the licensor.

Funding

This research did not receive any specific grant from funding agencies in the public, commercial, or not-for-profit sectors.

CRedit authorship contribution statement

Zachary Feinstein: Conceptualization, Writing - Review & Editing. Stefan Weber: Conceptualization, Writing - Review & Editing; Justin Plückebaum: Data Curation, Methodology, Software, Investigation, Writing - Original draft preparation.

References

- [1] Carlos F. Daganzo. “The cell transmission model: A dynamic representation of highway traffic consistent with the hydrodynamic theory”. *Transportation Research Part B: Methodological* 28 (4) (1994), pp. 269–287. DOI: 10.1016/0191-2615(94)90002-7.
- [2] Carlos F. Daganzo. “The cell transmission model, part II: Network traffic”. *Transportation Research Part B: Methodological* 29 (2) (1995), pp. 79–93. DOI: 10.1016/0191-2615(94)00022-r.
- [3] Ajith Muralidharan, Gunes Dervisoglu & Roberto Horowitz. “Freeway traffic flow simulation using the link node cell transmission model”. *2009 American Control Conference*. IEEE, 2009, pp. 2916–2921.
- [4] Gabriel Gomes et al. “Behavior of the cell transmission model and effectiveness of ramp metering”. *Transportation Research Part C: Emerging Technologies* 16 (4) (2008), pp. 485–513.
- [5] Md Hadiuzzaman & Tony Z Qiu. “Cell transmission model based variable speed limit control for freeways”. *Canadian Journal of Civil Engineering* 40 (1) (2013), pp. 46–56.
- [6] Ludovica Adacher & Marco Tiriolo. “A macroscopic model with the advantages of microscopic model: A review of Cell Transmission Model’s extensions for urban traffic networks”. *Simulation Modelling Practice and Theory* 86 (2018), pp. 102–119. DOI: 10.1016/j.simpat.2018.05.003.
- [7] JP Lebacque & MM Khoshyaran. “First order macroscopic traffic flow models for networks in the context of dynamic assignment”. *Transportation Planning: State of the Art*. Springer, 2002, pp. 119–140.
- [8] Isaak Yperman. “The link transmission model for dynamic network loading” (2007).
- [9] Gunnar Flötteröd & Jannis Rohde. “Operational macroscopic modeling of complex urban road intersections”. *Transportation Research Part B: Methodological* 45 (6) (2011), pp. 903–922.
- [10] Ping Wang. “Conditional cell transmission model for two-way arterials in oversaturated conditions”. PhD thesis. University of Alabama Libraries, 2010.
- [11] Tobias Pohlmann. “New Approaches for Online Control of Urban Traffic Signal Systems”. Dissertation. Braunschweig, Germany: Technische Universität, 2010.
- [12] Gunes Dervisoglu et al. “Automatic calibration of the fundamental diagram and empirical observations on capacity”. *Transportation Research Board 88th Annual Meeting*. Vol. 15. TRB Washington. 2009, pp. 31–59.
- [13] Yibing Wang et al. “Macroscopic traffic flow modelling of large-scale freeway networks with field data verification: State-of-the-art review, benchmarking framework, and case studies using METANET”. *Transportation Research Part C: Emerging Technologies* 145 (2022), p. 103904.
- [14] Michael James Lighthill & Gerald Beresford Whitham. “On kinematic waves II. A theory of traffic flow on long crowded roads”. *Proceedings of the Royal Society of London. Series A*.

- Mathematical and Physical Sciences* 229(1178) (1955), pp. 317–345. DOI: 10.1098/rspa.1955.0089.
- [15] Paul I. Richards. “Shock Waves on the Highway”. *Operations Research* 4(1) (1956), pp. 42–51. DOI: 10.1287/opre.4.1.42.
- [16] Martin Treiber & Arne Kesting. “Traffic flow dynamics”. *Traffic Flow Dynamics: Data, Models and Simulation*, Springer-Verlag Berlin Heidelberg 227 (2013), p. 228.
- [17] Tobias Pohlmann & Bernhard Friedrich. “Online control of signalized networks using the Cell Transmission Model”. *13th International IEEE Conference on Intelligent Transportation Systems*. IEEE, 2010. DOI: 10.1109/itsc.2010.5625064.
- [18] Xiang Li & Jian-Qiao Sun. “Multi-objective optimal predictive control of signals in urban traffic network”. *Journal of Intelligent Transportation Systems* 23(4) (2019), pp. 370–388.
- [19] “Forschungsgesellschaft für Strassen und Verkehrswesen”. *FSGV Verlag GmbH, Köln* (2001).
- [20] Gunnar Flötteröd & Gregor Lämmel. “Bidirectional pedestrian fundamental diagram”. *Transportation Research Part B: Methodological* 71 (2015), pp. 194–212. DOI: 10.1016/j.trb.2014.11.001.
- [21] Laura Munoz et al. “Methodological calibration of the cell transmission model”. *Proceedings of the 2004 American Control Conference*. IEEE, 2004. DOI: 10.23919/acc.2004.1383703.
- [22] Vincenzo Punzo & Marcello Montanino. “Speed or spacing? Cumulative variables, and convolution of model errors and time in traffic flow models validation and calibration”. *Transportation Research Part B: Methodological* 91 (2016), pp. 21–33.
- [23] Fo Vo Webster. *Traffic signal settings*. Tech. rep. 1958.
- [24] Anupam Srivastava, Wen-Long Jin & Jean-Patrick Lebacque. “A modified Cell Transmission Model with realistic queue discharge features at signalized intersections”. *Transportation Research Part B: Methodological* 81 (2015), pp. 302–315. DOI: 10.1016/j.trb.2015.05.013.